Sensitization of Er³⁺ emission at 1.5 μm by Yb³⁺ in KYb(WO₄)₂ single crystals

X. Mateos, M. C. Pujol, F. Güell, R. Solé, Jna. Gavaldà, M. Aguiló, F. Díaz, and J. Massons*

Laboratori de Física i Cristal·lografia de Materials (FiCMA) and IEA, Universitat Rovira i Virgili, 43005 Tarragona, Spain

We present our recent achievements in the growth and spectroscopic characterization of KYb(WO₄)₂ crystals doped with erbium ions (hereafter KYbW:Er). We grew single crystals of KYbW:Er at several erbium concentrations with optimal crystalline quality by the top-seeded-solution growth (TSSG) slow-cooling method. We carried out spectroscopic measurements related to the polarized optical absorption and optical emission at room temperature (RT) and low temperature (6 K). The splitting of the excited energy levels and the ground energy level of erbium in KYbW were determined, derived from the absorption and emission measurements at 6 K, respectively. We determined the near infrared, around 1.5 μm (6667 cm⁻¹), emission channels from the emission spectrum, and used the reciprocity method to calculate a maximum emission cross section of 2.7×10^{-20} cm² for the polarization parallel to the N_m principal optical direction for the 1.534 μm (6519 cm⁻¹) infrared emission. We measured the lifetime of the $^2F_{5/2} \rightarrow {}^2F_{7/2}$ transition of ytterbium and the $^4I_{13/2} \rightarrow {}^4I_{15/2}$ transition of erbium at RT for several erbium concentrations. Finally, we present the Judd-Ofelt calculations for the KYbW:Er system.

I. INTRODUCTION

There is a great deal of interest today in compact lasers operating in the infrared, around 1.5 and 3 μm (6667 and 3333 cm⁻¹), for applications in, for example, optical communications, medicine, light detection and ranging (LIDAR), etc.[1,2] Of these, solid state lasers are preferred for most applications because they are rugged, relatively simple, and easy to use.[3,4] Diode-pumped solid-state lasers are clearly very efficient because of the easy availability of this type of diode emitting in the 0.55–1.9 μm (18 182–5263 cm⁻¹) spectral range.

Erbium is a natural choice for obtaining laser radiation in the near infrared region after diode pumping because of its 1.5 μm (6667 cm⁻¹) emission and long lifetime. The 1.5 μm (6667 cm⁻¹) erbium emission is comprised of a very efficient three-level laser system. Its absorption band between 0.9–1.1 μm (11 111–9091 cm⁻¹) is in the easily available diode-laser emission range, however, its low absorption cross section in the abovementioned spectral range limits pump efficiency. A sensitizer ion is needed to increase this and therefore make luminescence generation more efficient. Unlike erbium ions, ytterbium ions have a high absorption cross section in the abovementioned spectral range and a high-energy overlap between the $^4I_{11/2}$ excited energy level of erbium and the $^2F_{5/2}$ excited energy level of ytterbium. This results in a resonant energy transfer from ytterbium to erbium as we can see in many crystals and glasses.[5,6] With all these advantages, ytterbium is ideal as a sensitizer ion of erbium.

The low-temperature monoclinic phase of potassium rare-earth tungstates $KRE(WO_4)_2$, can be doped with optical active lanthanide ions, even at a high concentration level, to produce a possible solid-state laser material.[7] Tungstate hosts are the most efficient of all known inorganic laser materials for stimulating emission at small pumping energies.[8] $KRE(WO_4)_2$ hosts have a high nonlinear susceptibility of the third order, so they are promising Raman-active media.[9]

Stoichiometric ytterbium tungstate KYb(WO₄)₂ (hereafter KYbW) has interesting spectroscopic properties due to its high ytterbium concentration. KYbW doped with erbium can work efficiently to achieve 1.5 μm (6667 cm⁻¹) infrared emission via energy transfer from ytterbium to erbium ions.

In this paper we present the growth of KYbW doped with erbium single crystals and study the spectroscopic properties of erbium ions sensitized by ytterbium in KYbW. We studied the polarized optical absorption at room-temperature (RT) and 6 K, the near infrared photoluminescence around 1.5 μm (6667 cm⁻¹) also at RT and 6 K, and finally, the decay curves at several erbium concentrations. We used the reciprocity method to calculate the $^4I_{13/2} \rightarrow {}^4I_{15/2}$ emission cross section from the absorption cross section line shape. We include the Judd-Ofelt calculations of erbium in the KYbW:Er system.

II. EXPERIMENT

Single crystals of potassium-ytterbium double tungstates doped with erbium $KYb_{1-x}Er_x(WO_4)_2$ (KYbW:Er) were grown by the top-seeded-solution growth slow-cooling method (TSSG). $K_2W_2O_7$ was chosen as a solvent because it does not introduce impurity ions and because its melting point is relatively low.

We grew KYbW:Er with a binary solution composition of 11.5 mol % solute/88.5 mol % solvent. Platinum crucibles of 50 mm in diameter were used to prepare around 200 g of solution, and the appropiate quantities of K_2CO_3, Yb_2O_3, Er_2O_3, and WO_3 (Fluka, 99.9% pure) were decomposed in accordance with the composition of the crystals to obtain the monoclinic phase. Previous studies[10] of KGdW:Ln³⁺ crystal growth showed that parallelepipedic **b**-oriented seeds make the crystals grow faster than other crystallographic orientations and produce inclusion-free crystals. The nominal atomic concentration of erbium substituting ytterbium are 0.5, 1, 3, and 5 mol % in the solution. For all samples, the erbium concentration in the crystals was determined by

electron-probe microanalysis (EPMA) with Cameca SX 50 equipment and its distribution coefficient was determined by

$$K_{Er^{3+}} = \frac{[\text{mol } Er^{3+}/(\text{mol } Er^{3+} + \text{mol } Yb^{3+})]_{crystal}}{[\text{mol } Er^{3+}/(\text{mol } Er^{3+} + \text{mol } Yb^{3+})]_{solution}}. \quad (1)$$

KYbW has a monoclinic crystallographic structure with space group $C2/c$ and lattice parameters $a = 10.590(4)$ Å, $b = 10.290$ Å, $c = 7.478(2)$ Å, and $\beta = 130.7(2)°$.[11] The three principal optical directions of monoclinic KYbW are located as follows along the crystal. The principal optical axis with maximum refractive index N_g is at 19° with respect to the **c** crystallographic axis in the clockwise rotation, with the **b** positive axis pointing towards the observer. The principal optical axis with intermediate refractive index N_m is at 59.7° with respect to the **a** crystallographic axis, and N_g and N_m are in the **a-c** plane. Finally, the N_p principal optical axis is parallel to the **b** crystallographic axis. A more precise structural and optical characterization can be found in previous papers.[11,12] The optical quality polished samples in our study were prisms cut with their faces perpendicular to the three principal optical axes.

Polarized optical absorption spectra of a KYbW:Er sample with an erbium concentration of 3.9×10^{19} at/cm^3, were performed at RT and 6 K with polarized light parallel to the N_g, N_m, and N_p principal optical directions. The measurements were taken with a VARIAN CARY-5E-UV-VIS-NIR 500Scan Spectrophotometer and a Glan-Taylor polarizer. Cryogenic temperatures were obtained with a Leybold RDK 6-320 cycle helium cryostat.

The equipment for our photoluminescence experiments consisted of a BMI OPO pumped by the third harmonic of a seeded BMI SAGA YAG:Nd laser. Pulses of 15 mJ (7 ns of duration, 10 Hz repetition rate) were achieved with a gaussian beam profile. Fluorescence was dispersed through a HR460 Jobin Yvon-Spex monochromator (focal length 460 mm, $f/5.3$, spectral resolution 0.05 nm) and detected by a cooled Hamamatsu R5509-72 NIR photomultiplier. The unpolarized emission spectra were performed at RT and 6 K on the same sample as the one used for optical absorption studies. The luminescence signal was analyzed by a EG&G 7265DSP lock-in amplifier. Lifetime measurements of the $^4I_{13/2}$ energy level were taken at various erbium concentrations, with the averaging facilities of a computer controlled Tektronix TDS-714 digital oscilloscope.

The emission cross section of an optical transition can be calculated from the absorption cross section line shape at RT of a particular energy level using the reciprocity method.[13] In fact, there are several ways of calculating the emission cross section of an energetic transition.[14] Both absorption and emission processes are characterized by their absorption and emission cross sections (σ_{abs}, σ_e), respectively. From the energies and degeneracies of the upper and lower energy levels, it is possible to have a mathematical expression that contains a direct relationship between the two abovementioned cross sections and that can calculate the emission cross section. The reciprocity calculation is based on

$$\sigma_e(\nu) = \sigma_{abs}(\nu) \frac{Z_l}{Z_u} \exp\left[\frac{(E_{zl} - h\nu)}{kT}\right], \quad (2)$$

where σ_e is the emission cross section to be calculated as a function of the frequency (or the wavelength). The σ_{abs} is the absorption cross section obtained from the RT optical absorption, which in our case, is the optical absorption of erbium ($^4I_{15/2} \rightarrow ^4I_{13/2}$ transition). The E_{zl} refers to the "zero line," or the energy separation, derived from the crystal field component, which is between the lowest energy sublevel of the excited energy level (upper) and the lowest energy sublevel of the ground level (lower). K is Boltzman's constant and h is Planck's constant. Finally, Z_u and Z_l are the partition functions of the upper and lower energy levels, respectively, caculated from

$$Z_{u,l} = \sum_k d_k \exp[-E_k/(kT)], \quad (3)$$

where d_k and the E_k are the degeneracies and the energies of each sublevel of the upper and lower energy levels involved in the system, obtained from the 6 K optical absorption.

To compare emission cross sections, it is interesting to also calculate it in another way. The Füchbauer-Ladenburg (FL) method is also used to calculate the emission cross section of a transition as a function of the wavelength. This method uses the expression

$$\sigma_e(\lambda) = \frac{\lambda^4 I(\lambda)}{8\pi n^2 c \tau_f \int I(\lambda) d\lambda}, \quad (4)$$

where $I(\lambda)/\int I(\lambda) d\lambda$ is the normalized line shape function, which in our case, correspond to the $^4I_{13/2} \rightarrow ^4I_{15/2}$ transition of Er^{3+}; n is the refractive index, c is the vacuum speed of the light, and τ_f is the spontaneous fluorescence time. The FL method needs only the RT emission spectrum, while the reciprocity method needs the RT and 6 K optical absorption spectra and the 6 K emission spectrum.

We can use the Judd-Ofelt theory[15,16] to describe the radiative optical properties of lanthanides. This theory is a second-order approximation for studying the lanthanide one-photon f-f transition. The experimental oscillator strength f_{exp} for a particular absorption is calculated from

$$f_{exp} = \frac{2mc}{\alpha_f h N \bar{\lambda}^2} \Gamma_{JJ'}, \quad (5)$$

where m is the electron mass, α_f is the fine-structure constant, N is the number of active ions per unit volume, $\bar{\lambda}$ is the average wavelength of the $J \rightarrow J'$ transition (transition between two energy levels), and $\Gamma_{JJ'} = \int \alpha(\lambda) \partial\lambda$ is the integrated RT absorption. We took the average wavelength $\bar{\lambda}$ of transitions to be the center of gravity of the absorption bands.

The theoretical oscillator strength of the transitions f_{th} between f-f levels is given by the expression

$$f_{\text{th}} = \chi \left[\frac{8\pi^2 mc}{h} \right] \frac{1}{3\bar{\lambda}(2J+1)}$$

$$\times \sum_{k=2,4,6} \Omega_k |\langle 4f^N \alpha[SL]J \| U^\lambda \| 4f^N \alpha'[S'L']J' \rangle|^2,$$

(6)

where $\chi = (n^2+2)^2/9n$, and n is the refractive index. Ω_k are the intensity parameters and $\langle \| U^\lambda \| \rangle$ are the double-reduced matrix elements operators corresponding to the $J \rightarrow J'$ transition, which in our case is Er^{3+}. The matrix elements given by Weber *et al.* were used in the calculation.[17] The Judd-Ofelt parameters were calculated by fitting the measured oscillator strength to the theoretical oscillator strength with the least-squares method.

The Judd-Ofelt parameters can be used to calculate the radiative transition rates $A_{JJ'}$ for the excited levels with

$$A_{JJ'} = \chi \left[\frac{32\pi^3 c \alpha_f}{3\bar{\lambda}^3} \right] \frac{n^2}{(2J+1)} S_{JJ'}.$$

(7)

The radiative lifetime of an emitting state is related to the total spontaneous emission probability of all the transitions from this state by

$$\tau_{rJ} = 1 \Big/ \sum_{J'} A_{JJ'}.$$

(8)

The luminescence branching ratios of a transition are calculated from

$$\beta_{JJ'} = A_{JJ'} \Big/ \sum_{J'} A_{JJ'}.$$

(9)

We treated the contributions of each polarization configuration separately and calculated the Ω_k^i ($i = N_g$, N_m, or N_p) set by minimizing the differences $\Sigma_{J'}(f_{\text{exp}} - f_{\text{th}})^2$. The f_{th} values corresponding to each $J \rightarrow J'$ transition were calculated with the corresponding refractive indices n_g, n_m, and n_p of the KYbW matrix at the corresponding $\bar{\lambda}$ of the multiplet. As the experiment was unable to separate the RT optical absorption of some energy levels, we treated these multiplets as a single set for performing the Judd-Ofelt calculations.

The quality of each fit is characterized by the root-mean-square deviations of the least-squares fitting

$$\text{r.m.s.} = \left[\sum_{q=1}^{q} \frac{(S_{\text{exp}} - S_{\text{cal}})^2}{q-p} \right]^{1/2},$$

(10)

where S_{exp} and S_{cal} are the standard deviations, q is the number of transitions, and p is the number of parameters to calculate (normally three).

TABLE I. Details of crystal growth. (A) Experience number. (B) Er$_2$O$_3$/(Yb$_2$O$_3$ + Er$_2$O$_3$) ratio in the solution (mol %). (C) Cooling interval (K). (D) Crystal weight (g). (E) Crystal dimensions along the c direction (mm). (F) Crystal dimensions along the a* direction (mm). (G) Crystal dimensions along the b direction (mm). (N) Distribution coefficient [Eq. (1)].

A	B	C	D	E	F	G	N
1	0.1%	18	1.28	12	4.5	6	
2	0.5%	27	2.06	10.5	9	6	1.20
3	1%	19.5	1.30	11	6	5	1.07
4	3%	22	1.56	12	6	5	1.18
5	5%	23	1.81	13	7	6.5	1.20

III. RESULTS AND DISCUSSION

A. Crystal growth

We used the top-seeded-solution growth slow cooling method to prepare KYb$_{1-x}$Er$_x$(WO$_4$)$_2$ single crystals at various erbium concentrations. Seed orientation was **b** crystallographic direction,[11] and inclusion-free crystals were obtained from these experiments. The temperature gradient in the solution was 0.13 K/mm and the saturation temperature was between 1173 and 1178 K. Other crystal growth data are given in Table I. Previous studies[18] show that the dopant ions are located in the rare-earth crystallographic position of the host (*KRE*W, in our case *RE* = Yb). A distribution coefficient close to 1 means that the solute composition is conserved in the crystal. This allows us to obtain single crystals with a high compositional homogeneity. Information about the Er^{3+} concentration in the crystal obtained in experiment number 1 and its distribution coefficient is not available because this concentration is on the limit of detection of the EPMA technique. Table II shows the EPMA results. Figure 1 shows a photograph of a single crystal of KYbW:Er.

B. Optical absorption

Figures 2 and 3 show the RT optical absorption cross section with polarized light parallel to the principal optical axis ($E//N_g$, N_m, and N_p). The spectrum in Fig. 2 was realized in the 0.9–1.1 μm (11 111–9091 cm^{-1}) range which corresponds to the $^4I_{15/2} \rightarrow {}^4I_{11/2}$ transition of Er^{3+} and $^2F_{7/2} \rightarrow {}^2F_{5/2}$ transition of Yb^{3+}. The spectrum in Fig. 3 was realized in the 1.425–1.625 μm (7000–6150 cm^{-1}) range, which corresponds to the $^4I_{15/2} \rightarrow {}^4I_{13/2}$ transition of Er^{3+}. To check the maximum resolution, we used two different samples from the same single crystal. The samples used for the 0.9–1.1 μm (11 111–9091 cm^{-1}) spectral

TABLE II. EPMA results.

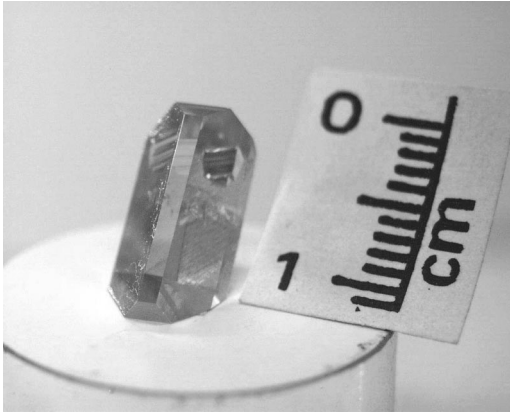| Exp. No.	[Er^{3+}] (at./cm^3)	Stoichiometric formula
2	3.9×10^{19}	KYb$_{0.994}$Er$_{0.006}$(WO$_4$)$_2$
3	7.1×10^{19}	KYb$_{0.99}$Er$_{0.01}$(WO$_4$)$_2$
4	2.3×10^{20}	KYb$_{0.965}$Er$_{0.035}$(WO$_4$)$_2$
5	3.9×10^{20}	KYb$_{0.94}$Er$_{0.06}$(WO$_4$)$_2$

FIG. 1. Photograph of a KYbW:Er single crystal grown by the TSSG slow cooling method.

range were therefore two very thin layers of about 50 μm (for all three polarizations) so as not to saturate the detector because of the high concentration of Yb^{3+} and the high absorption cross section that Yb^{3+} presents. On the other hand, the samples used to measure the optical absorption of the 1.425–1.625 μm (7018–6158 cm^{-1}) spectral range, were a prism 3.49 mm thick for the N_m and N_g optical directions and a prism of 3.22 mm thickness for the N_p optical direction. Both samples were from the same single crystal (experiment number 2). Figure 2 shows at RT the spectral region where the energy overlap and the energy transfer between erbium and ytterbium ions take place. Basically, all the absorption cross section that appears in the picture belongs to ytterbium because this ion is highly concentrate, it is a matrix constitutive ion, and the absorption cross section of ytterbium is higher than the absorption cross section of erbium in this spectral range. The maximum absorption cross section is about 11.6×10^{-20} cm^2 at 980.2 nm (10 202 cm^{-1}) for the polarization parallel to N_m principal optical direction. This agrees well with those published by Pujol *et al.* (Fig. 10, Ref. 12), and Kuleshov *et al.*,[19] where the samples were KYbW and KYW:Yb (5 % at.), respectively, and the absorption cross section was only due to Yb^{3+}. Figure 3 corresponds to the polarized optical absorption cross section of erbium at RT in the 1.424–1.625 μm (7000–6150 cm^{-1}) region with a maximum value of 2.6
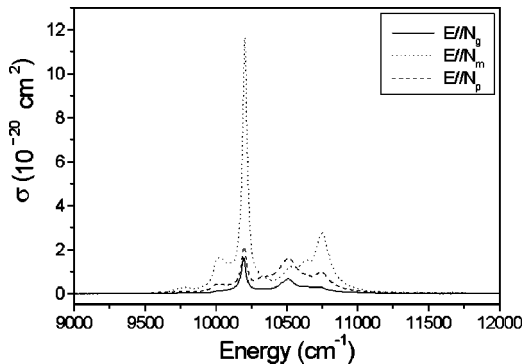

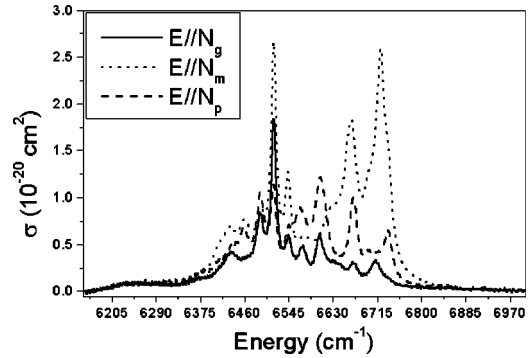FIG. 2. RT polarized optical absorption of KYbW:Er in the 0.9–1.1 μm range (11 111–9091 cm^{-1}).

FIG. 3. RT polarized optical absorption of erbium in KYbW in the 1.425–1.625 μm range (7018–6154 cm^{-1}).

$\times 10^{-20}$ cm^2 at 1.534 μm wavelength (6519 cm^{-1}), also for the polarization parallel to the N_m principal optical direction, which agrees well with the absorption cross section published by Kuleshov *et al.*[20] The absorption spectra show the anisotropy of the tungstates, which must be taken into account. The optical anisotropy of KYbW crystals is high, where the $E//N_m$ polarization is the most intense and $E//N_g$ is the least intense. This means that polarized stimulated emission will be possible in the future.

We performed complementary studies of polarized optical absorption at 6 K. We studied the optical absorption of KYbW doped with erbium in the 0.3–1.7 μm (33 300–5880 cm^{-1}) range at 6 K to determine the sublevels of all the possible excited energy levels caused by the elimination of the thermal population in the energy levels and the elimination of the thermal lattice vibrations. We assumed that at 6 K, only the lowest sublevel of the $^4I_{15/2}$ is populated in the case of erbium and that it is split by the local field of the ions surrounding the erbium dopant. The shape of the absorption lines should therefore reflect the transition probabilities from the lowest sublevel of the ground level to the sublevels of each excited energy levels of erbium. Figure 4 shows the polarized optical absorption spectra performed at 6 K of all the excited energy levels of erbium found in KYbW crystal, except the $^4I_{11/2}$ because it is overlapped with the $^2F_{5/2}$ level of ytterbium. The sample was the same as the one used at RT for the 1.425–1.625 μm (7018–6154 cm^{-1}) spectral range. The crystal field splits these manifolds into $(2J+1)/2$ sublevels according to the splitting expected by the crystalline field into the maximum number of Kramers levels (sublevels) due to the odd number of electrons of erbium and the low simmetry where erbium is located (C_2). Three aspects of the spectra are important to remark: first, the anisotropic contribution of the host was as above at RT, second, the optical transitions ($^4I_{15/2} \rightarrow ^4G_{11/2}$ and $^4I_{15/2} \rightarrow ^2H_{11/2}$) were hypersensitive due to the large oscillator strength (calculated later), and finally, the signal at 6 K was much more intense than the signals at RT. This was because at 6 K all the electronic population was in the lowest sublevel of the ground energy level, whereas at RT the electronic population was distributed among all the energy sublevels of the ground energy level. In this way, at 6 K, almost all the energy was concentrated in only one transition and this was more intense than at RT, where the energy was
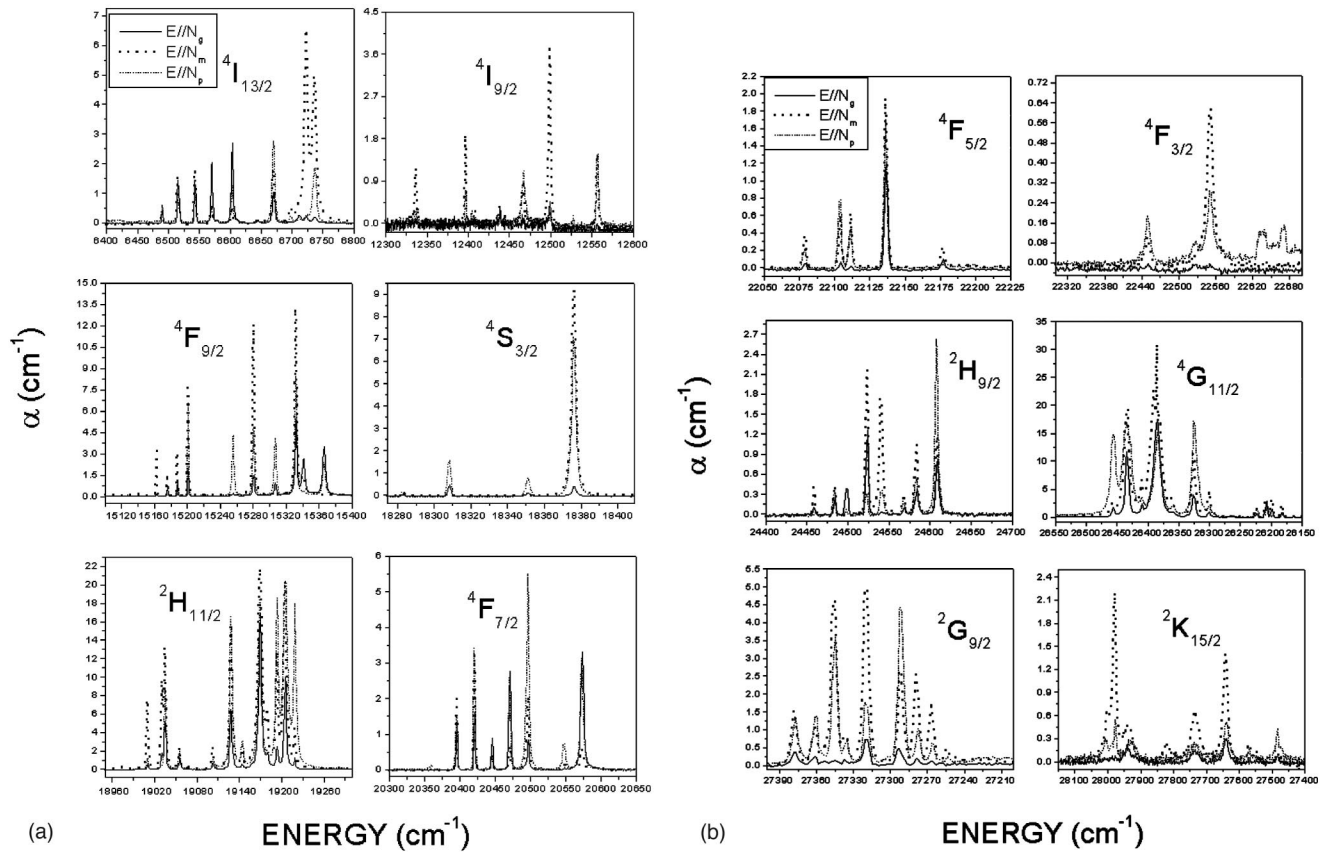
FIG. 4. 6 K polarized optical absorption of erbium in KYbW. (a) 1.563–0.484 μm (6400–20 650 cm^{-1}) range and (b) 0.454–0.365 μm (22 050–27 400 cm^{-1}) range.

distributed among several transitions, starting from the different energy sublevels of the ground energy level. This energy distribution among the different energy sublevels meant that at RT there was a broad band that did not exist at 6 K.

Table III shows the splitting of all the excited energy levels of erbium in KYbW single crystals. In all cases, the excited energy levels show the number of sublevels, which agrees very well with that expected from the maximum number of Kramers levels derived from the interaction of the ions with the crystal field. In the case of the $^4I_{15/2} \rightarrow ^4I_{13/2}$ infrared transition, the number of sublevels expected is seven and the energy difference between the first and second energy sublevel is 28 cm^{-1}. This energy difference will be used later to calculate the splitting of the ground energy level.

Because erbium has an odd number of electrons in the $4f$ shell, no selection rules are expected for the polarization of the electronic transitions. This means that erbium does not present dichroism, i.e., the number of peaks and the energy position of the absorption peaks must not depend on the polarization of the incident light, but intensity variation of the peaks associated with the three polarizations is still possible. This was confirmed experimentally both in the spectra recorded at RT and in those recorded at 6 K.

We compared the energy position of the center of gravity of each multiplet of Er^{3+} in $KGd(WO_4)_2$ (KGW),[21] and KYbW hosts. We found that the difference between these centers of gravity was smaller in KYbW crystals. Similarly,

the splitting of each energy level into its sublevels was slightly greater in KYbW crystals than in KGW crystals. From these two observations we conclude that the crystal field of KYbW is stronger than in KGW, which agrees well with smaller interatomic distances[22] Yb-Yb presented in KYbW than[11] the distances Gd-Gd, presented in KGW.[18] Also, the Judd-Ofelt parameters of erbium in KYbW (calculated later) and those of KGW,[21] showed the influence of this crystal field, in which the Judd-Ofelt parameters of KYbW were larger than those of KGW.

We used the reciprocity method to calculate the emission cross section for all three polarizations of the $^4I_{13/2} \rightarrow ^4I_{15/2}$ transition, from the absorption cross section spectra at RT. In this way, from the $^4I_{15/2} \rightarrow ^4I_{13/2}$ RT polarized optical absorption spectra, we calculated the polarized emission cross section of the $^4I_{13/2} \rightarrow ^4I_{15/2}$ transition using Eq. (2). The spectra are shown in Fig. 5, and the spectral range is 1.425–1.625 μm (7018–6154 cm^{-1}). The maximum absorption cross section, as mentioned above, for the polarization parallel to the N_m principal optical direction, which corresponds to the 1.534 μm (6519 cm^{-1}) signal, was about 2.6×10^{-20} cm^2. This absorption cross section is derived from Eq. (2) in a calculated emission cross section of 2.7 $\times 10^{-20}$ cm^2, which is similar to those published by Kuleshov *et al.*[20] The maximum calculated emission cross section correspond to the 1.534 μm (6519 cm^{-1}) energy position, which, as we will see in the next section, was close to the one found experimentally.

TABLE III. Splitting of the excited energy levels of Er^{3+} in KYbW single crystal obtained at 6 K.

$^{2s+1}L_j$		FWHM (cm^{-1}) (6 K)			$\int \alpha d\lambda$ (RT)		
		N_g	N_m	N_p	N_g	N_m	N_p
$^4I_{13/2}$	6517.2	3.26	3.39	3.75	16.7	38.4	21.2
	6545.1	2.63	2.77	0.02			
	6569.9	2.73	2.93	3.29			
	6603.0	3.14	3.53	2.07			
	6670.0	4.11	4.58	4.20			
	6723.2	4.81	6.52	4.72			
	6736.6	5.96	7.31	6.56			
$^4I_{9/2}$	12 336	1.44	2.47	4.05	0.1	2.1	1.8
	12 441		1.37	2.04			
	12 468	2.49	3.60	4.63			
	12 498	3.10	2.76	2.45			
	12 556	2.19	2.89	2.65			
$^4F_{9/2}$	15 176	0.09	1.31		3.9	10.8	5.9
	15 201	0.54	0.97	0.73			
	15 280	2.32	2.06	2.18			
	15 332	2.64	2.58	2.61			
	15 366	3.98		4.14			
$^4S_{3/2}$	18 308	1.60	1.63	1.53	0.3	1.9	0.9
	18 376	2.10	2.22	2.12			
$^2H_{11/2}$	19 035		2.96	2.48	10.0	63.6	31.9
	19 056	2.50	3.01	2.86			
	19 128	3.03	3.63	3.97			
	19 170	4.16	6.55	4.95			
	19 205	2.97	4.58	6.70			
	19 219	2.70	2.67	3.83			
$^4F_{7/2}$	20 421	2.09	1.97	1.68	1.7	3.6	1.8
	20 471	2.20	2.22	2.34			
	20 497	3.27	3.18	3.66			
	20 573	4.48	4.91	4.33			
$^4F_{5/2}$	22 104	1.77	1.52		$^4F_{5/2} + {}^4F_{3/2}$		
	22 136	1.75	1.80		0.4	1.3	0.4
	22 177	2.95	2.78				
$^4F_{3/2}$	22 450		5.93				
	22 551		10.81				
$^2H_{9/2}$	24 484	2.22	2.62	2.46	0.3	1.2	0.4
	24 523	2.87	2.97	2.61			
	24 540	0.61	2.92	2.23			
	24 569	2.86	3.50	3.28			
	24 609	2.99	3.31	3.40			
$^4G_{11/2}$	26 208	2.36	2.31	3.17	12.9	68.6	34.1
	26 223	2.42	3.17	3.13			
	26 326	4.69	5.29	8.86			
	26 386	11.35	14.79	11.37			
	26 434	5.78	9.60	15.55			
	26 457	3.95	3.07	8.14			

TABLE III. (*Continued.*)

$^{2s+1}L_j$	FWHM (cm^{-1}) (6 K)				$\int \alpha d\lambda$ (RT)	
	N_g	N_m	N_p	N_g	N_m	N_p
$^4G_{9/2}$				$^4G_{9/2} + {}^2K_{15/2}$		
27 293	4.60	2.90	4.36			
27 320	4.12	3.65	3.43	0.9	6.1	7.6
27 345	4.22	3.96	3.56			
27 361	4.47	4.21	3.92			
27 378	5.13	4.54	4.42			
$^2K_{15/2}$						
27 484	40.48	28.03	21.95			
27 568			47.62			
27 641	17.57		18.01			
27 735	33.29	28.03	58.11			
27 936		29.15				
27 978		10.76	7.78			
28 000		24.66	26.86			

C. Luminescence

RT and 6 K photoluminescence of erbium were achieved after a selective Yb^{3+} excitation at 940 nm (10 638 cm^{-1}) where no absorption of erbium takes place. The sample was KYbW:Er (3.9×10^{19} at./cm^3).

Figure 6 compares the experimental unpolarized infrared emission ($^4I_{13/2} \rightarrow {}^4I_{15/2}$ transition) with the spectrum calculated with the reciprocity method by taking into account the average of the three spectra for each polarization and the spectrum calculated with the FL method. We rescaled the experimental spectrum to match the calculated spectra and compare its shape. As the figure shows, all three spectra are very similar, except at short wavelengths because the reabsorption effect is greater and the reciprocity method does not consider this.

We performed systematic studies of photoluminesce of erbium at low temperature to determine the 1.5 μm (6667 cm^{-1}) emission channels and the splitting of the ground energy level of erbium. Figure 7 shows the 6 K emission corresponding to the $^4I_{13/2} \rightarrow {}^4I_{15/2}$ transition. The number of sublevels expected by the maximum number of Kramers levels due to the effect of the crystal field is eight. These clearly appear in the spectrum and are represented by crosses. The energy values of these eight signals are 6517, 6491, 6456, 6411, 6379, 6278, 6219, and 6206 cm^{-1}. The spectrum also shows minor peaks, which are represented by circles in the spectrum. These may be related to the transition from the second sublevel of the $^4I_{13/2}$ to the sublevels of the ground level. These peaks are displaced in accordance with the difference in energy between the first and second sublevels of the excited $^4I_{13/2}$ ($\Delta E = 28$ cm^{-1}, see Table III). From this, we know the energy position of the energy sublevels of
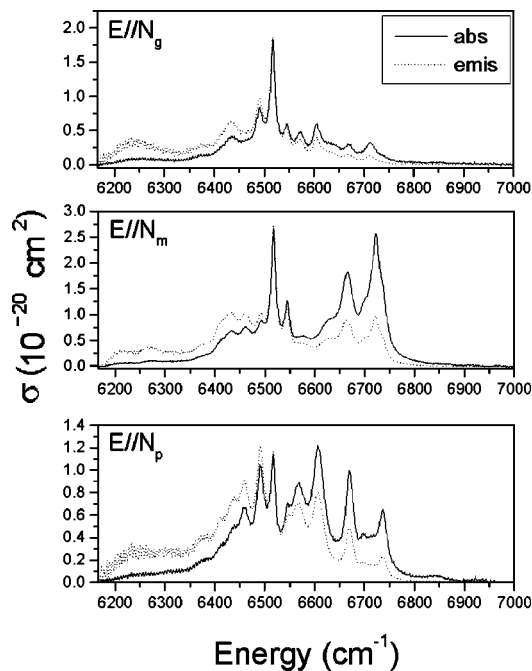

FIG. 5. Calculated emission cross section for the three polarizations of the $^4I_{13/2} \rightarrow {}^4I_{15/2}$ transition by the reciprocity method.
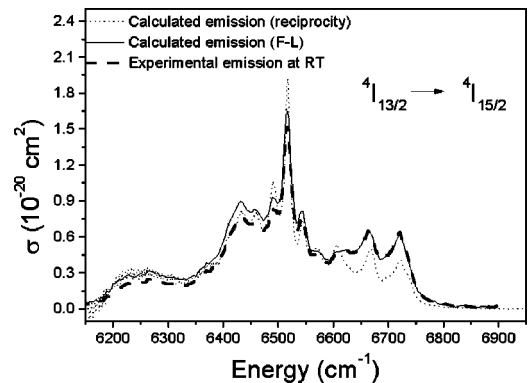

FIG. 6. Comparison of the emission cross section of the $^4I_{13/2} \rightarrow {}^4I_{15/2}$ transition, between the unpolarized calculated by the reciprocity and the Füchtbauer-Ladenburg methods and the experimental spectrum.
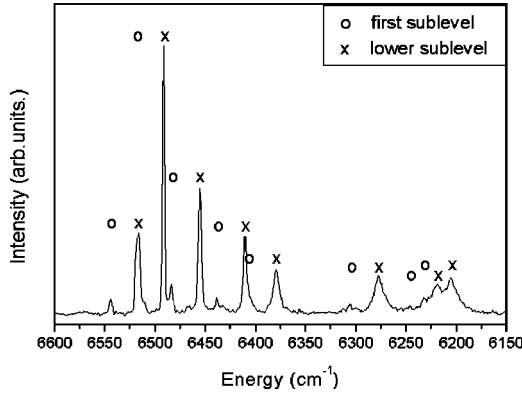
FIG. 7. 6 K emission spectrum of the $^4I_{13/2} \rightarrow ^4I_{15/2}$ transition of erbium in KYbW.

FIG. 9. Schematized energy transfer mechanism between erbium and ytterbium.

the ground. From the energy positions corresponding to the $^4I_{13/2}$ sublevels (see Table III) and by substracting the abovementioned energy values of emission signals, we obtained the splitting of the ground energy sublevel of erbium. The values were 0, 26, 61, 106, 138, 239, 298, and 311 cm^{-1}, and are very similar to those published in other tungstate matrices such as KGW, KYW, and KErW.[23] We found all of these values in a previous study also of an erbium doped KYbW crystal, by analyzing the green emission channels,[24] where the transition was $^4S_{3/2} \rightarrow ^4I_{15/2}$. By doing this we also found the splitting of the ground level of erbium, which was very close to the one we found in this study, where the infrared transition was $^4I_{13/2} \rightarrow ^4I_{15/2}$. We used these results to schematize the emission channels around 1.5 μm (6667 cm^{-1}) and the energy position of all the sublevels of the ground level in Fig. 8.

The above results are explained with the model in Fig. 9. The 1.5 μm (6667 cm^{-1}) emission can be attributed to a transition from the excited energy level of erbium $^4I_{13/2}$ to the ground $^4I_{15/2}$ level. A selective Yb^{3+} excitation at 940 nm (10 638 cm^{-1}) excites electrons from the ground energy level of ytterbium to the $^2F_{5/2}$ excited energy level. After excitation, they decay radiatively to the ground state or transfer part of their energy to the $^4I_{11/2}$ energy level of erbium by cross relaxation due to the energetic overlap between these two ions. Once erbium is excited, either a very fast nonradiative decay from $^4I_{11/2}$ to $^4I_{13/2}$ energy levels takes
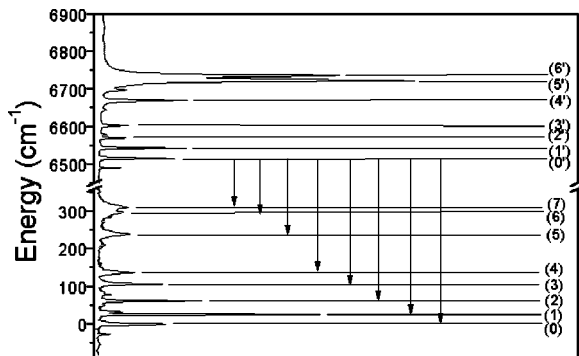
place, or the decay is radiative, emitting the near 3 μm (3333 cm^{-1}) emission ($^4I_{11/2} \rightarrow ^4I_{13/2}$ transition). From the $^4I_{13/2}$ energy level, the decay is mainly radiative to the ground state [infrared emission around 1.5 μm (6667 cm^{-1})]. Moreover, the electronic population of the $^4I_{11/2}$ energy level can be excited to the $^4F_{7/2}$ by a resonant absorption of a second pump photon. This phenomenon is widely known as two-photon absorption and is one type of step up-conversion mechanism.[25] Then, the up-conversion mechanism reduces the electronic population of the $^4I_{11/2}$ energy level and consequently the electronic population of the $^4I_{13/2}$ energy level, reducing the $^4I_{13/2}$ lifetime.

D. Lifetime measurements

We measured the time decay of the emission corresponding to the $^4I_{13/2} \rightarrow ^4I_{15/2}$ transition at 1.534 μm (6519 cm^{-1}) at several Er^{3+} concentrations in KYbW single crystals. To have a proof of the energy transfer between the two ions, we measured the time decay of ytterbium ions ($^2F_{5/2}$ energy level) increasing the erbium concentration. We performed this experiment on a KYbW sample and on KYbW:Er samples with 3.9×10^{19}, 7.1×10^{19}, 2.3×10^{20}, and 3.9×10^{20} at./cm^3 of Er^{3+}. We achieved the decay profile of the infrared luminescence signal by exciting the sample resonantly to ytterbium at 940 nm (10 638 cm^{-1}) and positioning the monochromator at the wavelength of the maximum emission at 1.040 μm (9615 cm^{-1}). Table IV shows that

FIG. 8. Schematized 6 K emission channels of erbium around 1.5 μm (6667 cm^{-1}).

TABLE IV. Lifetime of ytterbium ($^2F_{5/2}$) and erbium ($^4I_{13/2}$) as a function of the erbium concentration.

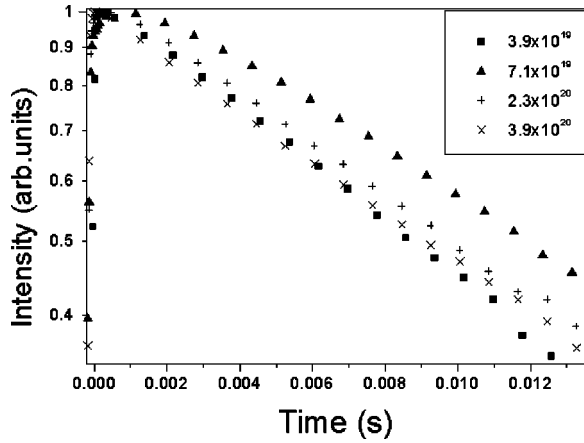| Erbium concentration (at./cm^3)	Yb($^2F_{5/2}$) lifetime (μs)	Er($^4I_{13/2}$) lifetime (ms)
0	600	
3.9×10^{19}	535	13.4
7.1×10^{19}	390	18.8
2.3×10^{20}	185	13.6
3.9×10^{20}	77	12.7

FIG. 10. Decay curves of the $^4I_{13/2} \to {}^4I_{15/2}$ transition in KYbW at different erbium concentrations.

when the erbium concentration increased, the ytterbium lifetime decreased. This fact indicated that part of the energy of ytterbium was transferred to erbium.

To study the lifetime of the $^4I_{13/2}$ level and its dependence on the Er^{3+} concentration, we performed the experiment on the same KYbW:Er samples. The decay curves were obtained after excitation to ytterbium at 940 nm (10 638 cm^{-1}) and positioning the monochromator at the wavelength of the maximum emission at 1.534 μm (6519 cm^{-1}). Figure 10 shows (in a semilogarithmic scale), the decay curves of the $^4I_{13/2} \to {}^4I_{15/2}$ transition of erbium at several erbium concentrations. From the decay curves, we can derive the lifetimes for all erbium concentrations (see Table IV). The lifetime increases until an erbium concentration of 7.1×10^{19} at./cm^3 due to the increase of the energy transfer. At higher erbium concentrations, the lifetime decreases significantly. This may be due to two possible mechanisms. The first one is the quenching phenomenon: when the erbium concentration increases, the Er-Er distances decrease, which increases the nonradiative energy transfer between erbium ions. This is reflected in a lower lifetime. In the second mechanism, the up-conversion process increases its probability and the energy to the $^4I_{13/2}$ energy level decreases. This is also reflected in the lifetime. The decay curves are single exponential, so non-radiative processes are not very important for the $^4I_{13/2}$ emission.

TABLE VI. Judd-Ofelt coefficients.

	$\Omega_2 \times 10^{20}$ (cm^2)	$\Omega_4 \times 10^{20}$ (cm^2)	$\Omega_6 \times 10^{20}$ (cm^2)
N$_g$	5.54	0.91	1.31
N$_m$	34.19	4.49	2.75
N$_p$	16.80	4.36	1.35

E. Judd-Ofelt calculations

We did the Judd-Ofelt analysis with the experimentally measured oscillator strength from the RT polarized optical absorption of the Er^{3+}-doped KYbW system. From Eq. (5), we determined the experimental oscillator strength and from Eq. (6), we determined the theoretical oscillator strength. Table V shows the slight differences in the values of the oscillator strengths.

We have treated the contributions of each polarization configuration separately. Table VI shows the Judd-Ofelt parameters (Ω_k^i, $i = N_g$, N_m, or N_p) for each polarization. These parameters agree well with those for other tungstates such as KGW (Ref. 21) and KYW (Ref. 20) although they are slightly bigger due to the previously mentioned influence of the crystal field.

We used these parameters to calculate the radiative transition probabilities (A_{ij}), the branching ratios (β_{ij}), and the radiative lifetimes (τ_r) (see Table VII). Subscripts i and j represent the different energy levels of Er^{3+}, as indicated in Fig. 10.

IV. CONCLUSIONS

We successfully grew KYb(WO$_4$)$_2$ single crystals doped with several concentrations of erbium ions by the TSSG method. We performed the spectroscopic characterization of erbium in this host, and measured the polarized optical absorption and the optical emission at room temperature (RT) and at low temperature (6 K). We also measured the lifetime of the 1.5 μm (6667 cm^{-1}) emission at RT for several erbium concentrations and we have made the Judd-Ofelt calculations for the KYbW:Er system.

From the polarized RT optical absorption measurements we calculated the estimulated emission cross section with the reciprocity method and the Füchtbauer-Ladenburg method.

TABLE V. Oscillator strength.

$^{2S+1}L_J$	$f_{exp} \times 10^6$			$f_{th} \times 10^6$		
	N$_g$	N$_m$	N$_p$	N$_g$	N$_m$	N$_p$
$^4I_{13/2}$	2.2132	5.0889	2.8095	1.9973	4.7076	2.4871
$^4F_{9/2}$	2.7293	7.6167	4.1962	2.4776	8.0162	6.2556
$^4S_{3/2}$	0.2729	1.8947	0.9575	0.8056	1.6194	0.7703
$^2H_{11/2}$	11.0708	70.6222	35.4221	12.9635	74.1010	37.4546
$^4F_{7/2}$	2.1625	4.6311	2.2903	3.0058	7.1805	4.3164
$^4F_{5/2} + {}^4F_{3/2}$	0.6574	1.9723	0.6126	1.5988	3.2004	1.5113
$^2H_{9/2}$	0.6210	2.2649	0.7489	1.2370	2.6495	1.3894
$^4G_{11/2}$	27.0592	144.0785	71.5980	24.8721	140.2153	69.5823
$^4G_{9/2} + {}^2K_{15/2}$	2.0436	13.9839	17.5201	2.8102	10.4914	7.0316

TABLE VII. Radiative properties of erbium in KYbW.

	λ (nm)	Energy (cm^{-1})	$A_{JJ'}$(s^{-1})	$\beta_{JJ'}$(%)	$\tau_{rad}(\mu s)$
$^2K_{15/2} \rightarrow {}^4G_{9/2}$	31 948.9	313	0.001	0	120
$^4G_{11/2}$	7987.2	1252	2.256	0.02	
$^2H_{9/2}*({}^4F_{9/2}+{}^4G_{9/2})$	3246.8	3080	25.534	0.3	
$^4F_{3/2}$	1951.6	5124	0.008	0	
$^4F_{5/2}$	1818.2	5500	4.954	0.05	
$^4F_{7/2}$	1404.9	7118	0.089	0	
$^2H_{11/2}$	1180.8	8469	868.414	10.42	
$^4S_{3/2}$	1076.0	9294	1.703	0.02	
$^4F_{9/2}$	812.5	12 307	192.966	2.31	
$^4I_{9/2}$	659.1	15 173	1221.135	14.65	
$^4I_{13/2}$	475.9	21 014	210.71	2.52	
$^4I_{15/2}$	361.8	27 639	5801.973	69.65	
$^4G_{9/2} \rightarrow {}^4G_{11/2}$	10649.6	939	0.454	0	6.5
$^2H_{9/2}*({}^4F_{9/2}+{}^4G_{9/2})$	3614.0	2767	7.123	0	
$^4F_{3/2}$	2078.6	4811	47.858	0.03	
$^4F_{5/2}$	1927.9	5187	267.232	0.17	
$^4F_{7/2}$	1469.5	6805	2132.251	1.38	
$^2H_{11/2}$	1226.1	8156	553.292	0.35	
$^4S_{3/2}$	1112.2	8991	236.221	0.15	
$^4F_{9/2}$	833.8	11 994	6058.255	3.92	
$^4I_{9/2}$	672.9	14 860	232.301	0.15	
$^4I_{13/2}$	483.1	20 701	128 810.726	83.49	
$^4I_{15/2}$	366.0	27 326	15 922.677	10.32	
$^4G_{11/2} \rightarrow {}^2H_{9/2}*({}^4F_{9/2}+{}^4G_{9/2})$	5470.5	1828	17.734	0	4.1
$^4F_{3/2}$	2582.6	3872	6.698	0	
$^4F_{5/2}$	2354.0	4248	9.844	0	
$^4F_{7/2}$	1704.7	5866	203.323	0.08	
$^2H_{11/2}$	1385.6	7217	108.629	0.04	
$^4S_{3/2}$	1243.5	8042	109.18	0.04	
$^4F_{9/2}$	904.6	11 055	5478.237	2.24	
$^4I_{9/2}$	718.3	13 921	1972.508	0.8	
$^4I_{13/2}$	506.0	19 762	13 704.617	5.62	
$^4I_{15/2}$	379.0	26 387	222 121.403	91.13	
$^2H_{9/2}*({}^4F_{9/2}+{}^4G_{9/2}) \rightarrow {}^4F_{3/2}$	4892.4	2044	0.406	0	67.4
$^4F_{5/2}$	4132.2	2420	2.666	0.01	
$^4F_{7/2}$	2476.5	4038	82.625	0.55	
$^2H_{11/2}$	1855.6	5389	116.279	0.78	
$^4S_{3/2}$	1609.3	6214	1.478	0	
$^4F_{9/2}$	1083.8	9227	125.893	0.84	
$^4I_{9/2}$	826.9	12 093	324.466	2.18	
$^4I_{13/2}$	557.6	17 934	9220.305	61.99	
$^4I_{15/2}$	407.2	24 559	4997.351	33.6	
$^4F_{3/2} \rightarrow {}^4F_{5/2}$	26 595.7	376	0.097	0	158.8
$^4F_{7/2}$	5015.0	1994	2.748	0.04	
$^2H_{11/2}$	2989.5	3345	0.375	0	
$^4S_{3/2}$	2398.1	4170	50.765	0.8	
$^4F_{9/2}$	1392.2	7183	64.662	1.02	
$^4I_{9/2}$	995.1	10 049	1273.841	20.23	
$^4I_{13/2}$	629.3	15 890	389.19	6.18	
$^4I_{15/2}$	444.1	22 515	4513.098	71.69	

TABLE VII. (*Continued.*)

	λ (nm)	Energy (cm^{-1})	$A_{JJ'}$(s^{-1})	$\beta_{JJ'}$(%)	$\tau_{rad}(\mu s)$
$^4F_{5/2} \rightarrow {}^4F_{7/2}$	6180.5	1618	7.214	0.06	94.6
$^2H_{11/2}$	3368.1	2969	12.941	0.12	
$^4S_{3/2}$	2635.7	3794	8.715	0.08	
$^4F_{9/2}$	1469.1	6807	437.537	4.12	
$^4I_{9/2}$	1033.8	9673	510.12	4.81	
$^4I_{13/2}$	644.6	15 514	4633.577	43.73	
$^4I_{15/2}$	451.7	22 139	4985.451	47.05	
$^4F_{7/2} \rightarrow {}^2H_{11/2}$	7401.9	1351	5.441	0.03	69.7
$^4S_{3/2}$	4595.6	2176	0.152	0	
$^4F_{9/2}$	1927.2	5189	36.635	0.25	
$^4I_{9/2}$	1241.5	8055	529.551	3.68	
$^4I_{13/2}$	719.6	13 896	2248.44	15.64	
$^4I_{15/2}$	487.3	20 521	11 553.498	80.37	
$^2H_{11/2} \rightarrow {}^4S_{3/2}$	12 121.2	825	0.177	0	17.8
$^4F_{9/2}$	2605.5	3838	186.215	0.31	
$^4I_{9/2}$	1491.6	6704	675.24	1.14	
$^4I_{13/2}$	797.1	12 545	722.432	1.22	
$^4I_{15/2}$	521.6	19 170	57 177.331	97.3	
$^4S_{3/2} \rightarrow {}^4F_{9/2}$	3319.0	3013	1.895	0.03	176.2
$^4I_{9/2}$	1701.0	5879	208.776	3.67	
$^4I_{13/2}$	853.2	11 720	1504.804	26.51	
$^4I_{15/2}$	545.1	18 345	3959.601	69.77	
$^4F_{9/2} \rightarrow {}^4I_{9/2}$	3489.2	2866	33.368	0.54	163.8
$^4I_{13/2}$	1148.5	8707	316.542	5.18	
$^4I_{15/2}$	652.2	15 332	5754.63	94.26	
$^4I_{9/2} \rightarrow {}^4I_{13/2}$	1712.0	5841	152.722	18.35	1202.0
$^4I_{15/2}$	802.2	12 466	679.248	81.64	
$^4I_{13/2} \rightarrow {}^4I_{15/2}$	1509.4	6625	399.874	100	2500.8

The results agree very well with the literature in similar tungstate hosts. From the 6 K polarized optical absorption measurements, we determined the energy position of the sublevels of each excited energy levels.

From the RT optical emission, we compared the experimental emission line shape with those calculated with the reciprocity and FL methods. We consider these spectra to be close. From the 6 K optical emission of the $^4I_{13/2} \rightarrow {}^4I_{15/2}$ transition of erbium, we found the energy position of the sublevels of the ground level. The results also agree very well with those in the literature for similar tungstate hosts.

From the RT decay curves of the $^4I_{13/2} \rightarrow {}^4I_{15/2}$ transition of erbium, we calculated the lifetime of the $^4I_{13/2}$ energy level at several erbium concentrations.

*Author to whom correspondence should be addressed.

[1] J.A. Hutchinson and T.H. Allik, Appl. Phys. Lett. **10**, 1424 (1992).

[2] J. F. Digonnet, *Rare Earth Doped Fiber Lasers and Amplifiers* (Dekker, New York, 1993).

[3] W. Koechner, *Solid-State Laser Engineering*, 4th ed. (Springer-Verlag, Berlin, 1996).

[4] R. C. Powell, *Physics of Solid-State Laser Materials* (Springer-

Verlag, Berlin, 1998).

[5] K. Tamura, E. Yoshida, E. Yamada, and M. Nakazava, Electron. Lett. **32**, 835 (1996).

[6] E. Cantelar, J.A. Muñoz, J.A. Sanz-Garcia, and F. Cussó, J. Phys.: Condens. Matter **10**, 8893 (1998).

[7] P. Klopp, U. Griebner, V. Petrov, X. Mateos, M.A. Bursukova, M.C. Pujol, R. Solé, Jna. Gavaldà, M. Aguiló, F. Güell, J. Massons, T. Kirilov, and F. Díaz, Appl. Phys. B: Lasers Opt. **74**, 185 (2002).

[8] A.A. Kaminskii, H.R. Verdun, W. Koechner, F.A. Kuznetsov, and A.A. Pavlyuk, Kvantovaya Elektron. (Kiev) **19**, 941 (1992).

[9] A.A. Lagatsky, N.V. Kuleshov, and V.P. Mikhailov, Opt. Commun. **165**, 71 (1999).

[10] M.C. Pujol, R. Solé, V. Nikolov, Jna. Gavaldà, J. Massons, C. Zaldo, M. Aguiló, and F. Díaz, J. Mater. Res. **14**, 3739 (1999).

[11] M.C. Pujol, X. Mateos, R. Solé, J. Massons, Jna. Gavaldà, X. Solans, F. Díaz, and M. Aguiló, J. Appl. Crystallogr. **35**, 108 (2002).

[12] M.C. Pujol, M.A. Bursukova, F. Güell, X. Mateos, R. Solé, Jna. Gavaldà, M. Aguiló, J. Massons, F. Díaz, P. Klopp, U. Griebner, and V. Petrov, Phys. Rev. B **65**, 165121 (2002).

[13] S.A. Payne, L.L. Chase, L.K. Smith, W.L. Kway, and W.F. Krupke, IEEE J. Quantum Electron. **28**, 2619 (1992).

[14] W.F. Kupke, M.D. Shinn, J.E. Marion, J.A. Caird, and S.E. Stokowski, J. Opt. Soc. Am. B **3**, 102 (1986).

[15] B.R. Judd, Phys. Rev. **127**, 750 (1962).

[16] G.S. Ofelt, J. Chem. Phys. **37**, 511 (1962).

[17] M.J. Weber, Phys. Rev. **157**, 262 (1967).

[18] M.C. Pujol, R. Solé, V. Nikolov, J. Massons, Jna. Gavaldà, X. Solans, C. Zaldo, F. Díaz, and M. Aguiló, J. Appl. Crystallogr. **34**, 1 (2001).

[19] N.V. Kuleshov, Opt. Lett. **22**, 1317 (1997).

[20] N.V. Kuleshov, A.A. Lagatsky, A.V. Podlopensky, V.P. Mikhailov, A.A. Kornienko, E.B. Dunina, S. Hartung, and G. Huber, J. Opt. Soc. Am. B **15**, 1205 (1998).

[21] M.C. Pujol, M. Rico, C. Zaldo, R. Solé, V. Nikolov, X. Solans, M. Aguiló, and F. Díaz, Appl. Phys. B: Lasers Opt. **68**, 197 (1999).

[22] B.Z. Malkin, A.A. Kaminskii, N.R. Agalmayan, L.A. Bumagina, and T.I. Butaeva, Phys. Status Solidi B **111**, 417 (1982).

[23] A. A. Kaminskii, *Laser Crystals, Their Physics and Properties*, 2nd ed., Vol. 14 of *Springer Series in Optical Science* (Springer, Berlin, 1990).

[24] X. Mateos, F. Güell, M.C. Pujol, M.A. Bursukova, R. Solé, Jna. Gavaldà, M. Aguiló, F. Díaz, and J. Massons, Appl. Phys. Lett. **80**, 4510 (2002).

[25] P.E.A. Möbert, E. Heumann, G. Huber, and B.H.T. Chai, Opt. Lett. **22**, 1412 (1997).